Research in Astron. Astrophys. Vol.0 (20xx) No.0, 000–000
http://www.raa-journal.org *http://www.iop.org/journals/raa*
(LaTeX: 2020-0461.tex; printed on March 9, 2021; 15:01)

***R**esearch in*
***A**stronomy and*
***A**strophysics*

The research objectives and observational possibilities for fast moving Near-Earth Asteroids

Anton Pomazan[1,2], Zheng-Hong Tang[1], Nadiia Maigurova[3], Kai Tang[1], Yong Yu[1] and Yin-Dun Mao[1]

[1] Shanghai Astronomical Observatory, Chinese Academy of Sciences, Shanghai 200030, China; *antpomaz@shao.ac.cn*
[2] University of Chinese Academy of Sciences, Beijing 100049, China
[3] Research Institute Mykolaiv Astronomical Observatory, Mykolaiv 54030, Ukraine

Received 2020 December 15; accepted 2021 March 3

Abstract The paper describes observations of fast-moving near-Earth asteroids (NEAs) made with the small ground-based telescopes of National Time Service Center of Chinese Academy of Science (NTSC of CAS) and Research Institute Mykolaiv Astronomical Observatory (RI MAO) by the Rotating-drift-scan CCD (RDS CCD) technique. This technique used to obtain the point images of both the studied objects and reference stars. The results of ongoing follow-up observations of NEAs are discussed. As comparison with JPL ephemerides computed for these asteroids is shown, differences between the observed positions and JPL calculated positions were generally small, and the standard deviation scatter comparing these results were typically $(0.2'' - 0.3'')$ in both coordinates for objects with apparent velocity of which substantially exceed FWHM for exposure time. The results of comparative statistics of such observations from MPC database show that this is a good level of precision for NEAs. Moreover, the telescopes with implemented RDS CCD technique are observing the NEAs that are close approaching to the Earth and with enough observations can improve the precision of determining their orbital elements and impact predictions.

Key words: astronomical databases: miscellaneous — surveys — methods: observational — techniques: miscellaneous — astrometry — minor planets, asteroids: general

1 INTRODUCTION

Ground-based optical positional observations of the Solar System bodies are the basis for creation of the motion theories, defining and clarifying of the orbit elements and dynamic parameters. The regular observations of near-Earth objects (NEOs) are one of the most important aspects of studying the problem of asteroid-cometary hazard and allows us to do refinement of their orbits. It makes possible to predict a collision of such body with the Earth in future and to take appropriate measures in advance. Therefore, it becomes critically important to perform efficient follow-up observations. Nowadays, many scientific projects, which are allocated significant funding, are engaged in monitoring of known NEOs and the search for new ones. According to current information represented on International Astronomical Union (IAU) Minor Planet Center[1] (MPC) website more than 22,000 near-Earth asteroids (NEAs) are

[1]IAU MPC Database. Available online at: *https://www.minorplanetcenter.net*

known, including more 900 NEAs larger than 1 km in diameter. Recent investigations in sizefrequency distribution (SFD) and estimations the completion versus size of NEAs show almost full completion, from 990 (Harris & D'Abramo 2015) to 920 (Tricarico 2017) NEAs in sizes 1+km (which is considered equivalent to an absolute magnitude H equal or brighter than 17.75 mag at a nominal average geometric albedo $pV = 0.14$). In the same time, completion significantly decreasing for lower sizes. The total amount of small NEAs in simulations has been estimated as (7 2) 10^4 NEAs (Tricarico 2017) larger than 100 m (corresponding absolute magnitude $H < 22.75$ mag), or 3.5 10^6 (Trilling et al. 2017) for objects with $H \leq 27.3$ mag (around 10 m) and higher orders for smaller sizes.

Currently, there are quite a few asteroid surveys that work in the optical range. Among them are such surveys as the *Catalina Sky Survey* (CSS) (Larson et al. 1998), the *Pan-STARRS* (Wainscoat et al. 2018), restarted *NEOWISE* mission (Mainzer et al. 2014) (infrared space-based survey), and *ATLAS* (Tonry et al. 2018), which account for the bulk of the discoveries of new asteroids according to data in Jedicke et al. (2015). The number of new discovered objects grows each year[2]. But despite the efforts being made in this direction, the task of detection of all potential threats cannot be considered solved. Current amount of known small-sized NEAs is significantly larger than population estimated in simulations (Tricarico 2017; Trilling et al. 2017). Big expectations in discovering and reaching big part of completeness of NEOs and potentially hazardous asteroids (PHAs) populations are associated with the Large Synoptic Survey Telescope (LSST) (Jones et al. 2018).

The population of NEAs includes more than 2,000 PHAs for the Earth. Their minimum orbit intersection distance (MOID) is equal or less than 0.05 AU and diameters are more than 140 m (corresponding absolute magnitude $H < 22$ mag) which means they could result in the significant consequences and threat to life on Earth. Therefore, it is critically important to detect, identify and systematically monitoring such objects to determine the orbital elements with precision sufficient to predict the probability of terrestrial impact as part of Space Situational Awareness. As it shown in Maigurova et al. (2018) there is more than 40% of known PHAs discovered after they had approached on a minimum distance to the Earth.

The maximum close approach (CA) with the Earth is the most favorable for the searching of small-scale NEAs because at another time they have rather weak apparent magnitudes and require large-diameter telescopes for specific observations. At the same time, their apparent velocity increases significantly which decreases precision of positional observations. All current observations of PHAs since 2010 presented in the IAU MPC database (2020 March) with additional information from JPLs HORIZONS ephemeris system[3] were analyzed regarding apparent motion. The apparent motion has been calculated as square root of sum of squares of the angular rates of changes in apparent right ascension and declination which taken from JPLs HORIZONS ephemeris calculated at specified time moment. Extracted observations have been linked with 1494 known CA on a distance less 0.2 AU to the Earth for 1061 PHAs taken from the CNEOS. The observations which are in range 3 days to time moment of known CA were further analyzed. The Figure 1 shows the distribution of (O – C) differences of PHA positions such linked observations versus distance to the Earth in right ascension and declination. The (O – C) differences here mean residuals between observed (O) and ephemerid (C) positions of the objects. The plot shows strong dispersion and increasing standard deviation values of (O – C) differences of the observations with decreasing distance to the Earth and increasing apparent motion of the objects. This, respectively, indicates the difficulty of the observations of such objects. The mean apparent motion is $39''$ min^{-1} (15.6 deg day^{-1}) for observations at distances less than 0.06 AU to the Earth, at the same time, this part includes around 60% of observations. It should be noticed, there are only a few observations for 5 PHAs ((503941) *2003 UV11*, (357439) *2004 BL86*, (308635) *2005 YU55*, *2014 JO25*, *2015 TB145*) with apparent motion more $160''$ min^{-1} (64 deg day^{-1}) taken during specific international observational campaigns. Most of observations stop at high apparent motion due to difficulties with tracking of object in field of view (FOV) of telescope. Strong apparent motion can lead to effects of trailing losses, which will lead to a decreasing in new discoveries (Tricarico 2017). High

[2]Data from JPL Center for NEO Studies (CNEOS), *https://cneos.jpl.nasa.gov/stats/*

[3]JPL HORIZONS on-line solar system data and ephemeris computation service, *https://ssd.jpl.nasa.gov/?horizons*

speed of visible movement is one of the significant factors (Veres et al. 2018), which lead to the fact that some of the new discoveries of NEA remain unconfirmed and may be lost.

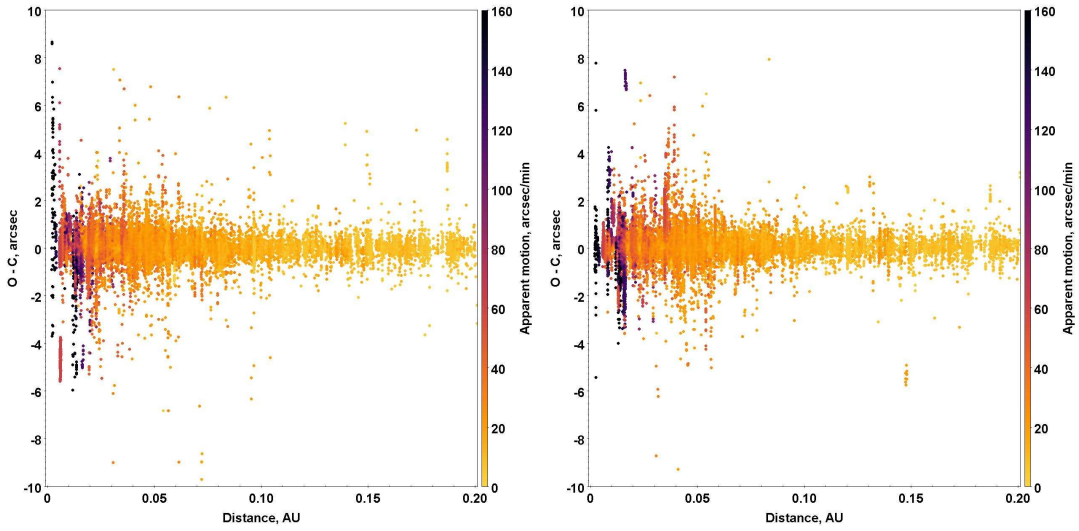

Fig. 1: Distribution of differences O-C in positions of PHA versus distances to Earth for observations taken in range 3 days to time moment of known CA fo right ascension (left) and declination (right).

This article presents one of the methods for conducting reliable and effective observations of the NEAs at the moment of CA to Earth, which was implemented on the telescope of the LiShan observation station (NTSC, China) and the KT-50 telescope (RI MAO, Ukraine). The main feature of Rotating-drift-scan CCD (RDS CCD) technique is usage of rotational platform and drift scan mode of CCD to obtain separate images of reference stars and objects for the positional observations of celestial bodies with high visible velocities. The usage this combined observational method allows us to get all celestial objects images as a point, that in turn to determine the coordinates of all image centers with sufficient precision.

Section 2 of this paper describes RDS CCD technique and telescopes where it has been implemented; Section 3 presents obtained NEAs observations and astrometric reductions; and in Section 4 positional precision with RDS CCD method is discussed on comparative statistics with other data from IAU MPC database.

2 ROTATING-DRIFT-SCAN CCD TECHNIQUE AND TELESCOPES

As it mentioned above, high apparent motion of object for required exposure time in FOV of telescope at CA to the Earth is main difficulty in observations of such objects. It makes impossible to obtain pointed images of reference stars and objects of interest simultaneously. The frames for reference stars and objects are obtained separately using the RDS CCD technique. The basic idea of combination the time delay integration (TDI) mode of CCD (Gehrels et al. 1990) with the rotation platform for observations of fast-moving NEAs was presented and discussed by researchers from Shanghai Astronomical Observatory (ShAO) and RI MAO in 2006 (Tang et al. 2006). The basic procedure of using RDS CCD technique to observe NEOs is described in Tang et al. (2014).

The TDI mode is usually used to imaging long continuous strips of the sky. The exposure time of classical TDI depends only on the speed of a target and field size which cant be changed (in full exposure time). Implemented RDS CCD technique uses specified exposures during which CCD camera works in TDI mode (speed of reading out matches with the speed of a target and pixel scale). When

the specified exposure time is finished readout process with maximum speed is started without CCD flushing (Shulga et al. 2008).

The CCD with TDI mode is installed on a rotating platform and rotates to make the direction of pixel reading line parallel to the motion direction of the object, the CCD then works in TDI mode with speed of pixel reading equal to apparent motion of object. It allows to get pointed images of moving objects. Considering the directions of the motion most of NEAs are usually close to those of the stars (according to distribution of inclinations to the ecliptic only 30% of all discovered NEAs have inclination more than 15 °), TDI mode can be used also to observe stars but with apparent sidereal velocity (15 $\cos(\delta)$) and short exposure time. The pointed images of stars will be obtained then as reference frames on separated frames from the object. It is necessary to read the lines of the CCD in perfect synchronization with the moving speed of the stars or object on the focal plane of telescope.

Such observational technique supposes get at least 3 frames as one set at the fixed telescope position. The telescope and CCD are locked after telescope is moved to a new target position and CCD is rotated to the appropriate direction of the apparent motion of the object. First and last frames in the set are reference with pointed images of stars, while middle one is taken to get pointed image of the object. Since the telescope keeps stable position during one set of observation the plate constants could be interpolated by linear function on short time interval (Kozyrev et al. 2010). Telescope and CCD are moved to a new position after all frames in the set have been taken. Additional requirement is the taking observations of objects with hour angles in range 1.5 h around meridian and zenith distances less 50 °, where are no very large astrometric errors caused by anomalous refraction.

The RDS CCD technique is implemented on two small-sized parallactic optical telescopes. The LiShan telescope is one of them. It belongs to observational station of NTSC of CAS at LiShan mountain, near to Xian city. The first test observations of NEAs have been done in 2018 October and regular observations have been started since second half of 2019. The IAU MPC observatory code has been applied in 2019 December and code O85 was designated for LiShan observational station of NTSC of CAS. According to agreement between National Time Service Center and ShAO, the part of observational time belongs to ShAO. The other one is KT-50 which is placed in RI MAO (IAU MPC Observatory code 089). The regular observations of selected asteroids and NEOs at KT-50 telescope have been used since 2011 (Ivantsov et al. 2012). Table 1 gives detailed technical characteristics about the telescopes and instrumental systems. Depending on the exposure time and apparent speed of motion of NEAs, the size of frames is different.

As is known, the accuracy of determination of the image center coordinates depends on the SNR and FWHM values (King 1983). The FWHM value does not depend on the brightness of the object and is determined only by the optical design and the location of the telescope. With the classical method of observations, in case the object moves at high apparent velocity in the FOV and requires long exposures, its images are stretched. This leads to the deterioration in accuracy when the obtained image is approximated by the PSF function. The average FWHM for a given telescope can be used as an indicator of the usage of the RDS CCD technique. If the apparent displacement of the object during the supposed exposure will exceed the FWHM value by several times, the usage of the RDS CCD technique is expedient. Such threshold value can be defined based on the selected approximation function of the PSF.

The advantage of the RDS CCD technique, especially at the limit of the telescope's capabilities, is the possibility of increasing the exposure time for faint objects, if their speed and direction of motion do not coincide with the diurnal motion of the stars. In this way, the usage of the RDS CCD technique for observations of such kind objects allows to keep pointed images of them, which gives both the higher SNR value and a possibility of a more accurate image center calculation, and, consequently, the equatorial coordinates.

3 NEA OBSERVATIONS PROCESSING

The processing pipeline for calculation of objects equatorial coordinates includes the next steps:

I) Standard astrometric data reduction of CCD frames with reference stars to calculate equatorial coordinates of optical centers, standard coordinates of reference stars and plate constants,

Table 1: Telescopes Technical Characteristics.

Telescope	LiShan telescope (NTSC)	KT-50 telescope (RI MAO)
Location	China, LiShan mountain	Ukraine, Mykolaiv
Coordinates (IAU MPC):		
Longitude, $^\circ E$	109.213	31.970
Latitude, $^\circ N$	34.353	46.972
Altitude, m	950	50
Diameter and type, m	0.50 Cassegrain	0.50 Maksutov
Focal length, mm	3445	3000
FWHM, $''$	2.3	2.5
CCD	Alta U9000	
Size, px	3056 x 3056	
Pixel size, mkm	12 x 12	
Scale, $''$ px^{-1}	0.72	0.83
FOV, $'$	36.7 x 36.7	42.5 x 42.5
Filter	without	Johnson V (since 2018)
Exposure, s		
Reference stars	10 – 15	10
Asteroids	25 – 100 for objects 14.5 17.0 mag	60 150 for objects 12 17.5 mag

II) Measurements of the asteroid rectangular coordinates in CCD frame;

III) Linear interpolation of obtained plate constants, equatorial coordinates of optical centers at the time associated with frame with the asteroid;

IV) Calculation of the asteroid equatorial coordinates.

The detailed description of the reduction pipeline algorithm of combined scheme is given in Sybiryakova et al. (2015).

The first step of processing, regarding to astrometric reductions of the reference frames has been carried out by the "Astrometrica" package[4] in automatic mode. No bias, dark and flatfield corrections were applied to the raw CCD frames before processing. According to Evans et al. (2002), resulting effect of applying flatfield corrections in TDI mode of CCD camera is negligible and might be ignored here. Other preprocessing corrections will have even less effect. The FOV of the telescopes and limiting magnitude allow to get a sufficient number of reference stars to perform astrometric data reductions with a 3rd order polynomial for transformations between rectangular and standard coordinates despite the fact of usage relatively short exposure time (10 - 15 s) for frames with reference stars. The limiting magnitude for LiShan telescope without optical filters is 18 mag, the one for KT-50 telescope is 16 mag with standard Johnson V filter. $GaiaDR2$ catalog is used as reference catalog to perform astrometric data reductions at the present time.

The dependences of a precision of a single observation of the stars of the reference system versus the G magnitude of $GaiaDR2$ system for the used telescopes are shown on Figure 2. The standard deviation of the (O – C) differences of stars positions is considered as an estimation of the precision, where O means observed position, C - stars position from $GaiaDR2$ catalog. As can be seen from the Figure 2 there are no significant deviations from zero point in (O – C) differences along represented magnitudes. Mean (O – C) values with standard deviation are $-0.01''$ $0.08''$ in right ascension and declination for LiShan telescope and $0.01''$ $0.10''$ and $0.01''$ $0.09''$ respectively for KT-50 telescope. A

[4] Astrometrica, *http://www.astrometrica.at*

noticeable decreasing in precision is for faint stars, therefore to perform reliable astrometric reductions stars in the range 12 - 17.0 mag for LiShan telescope and 11 - 15.0 mag for KT-50 telescope have been chosen.

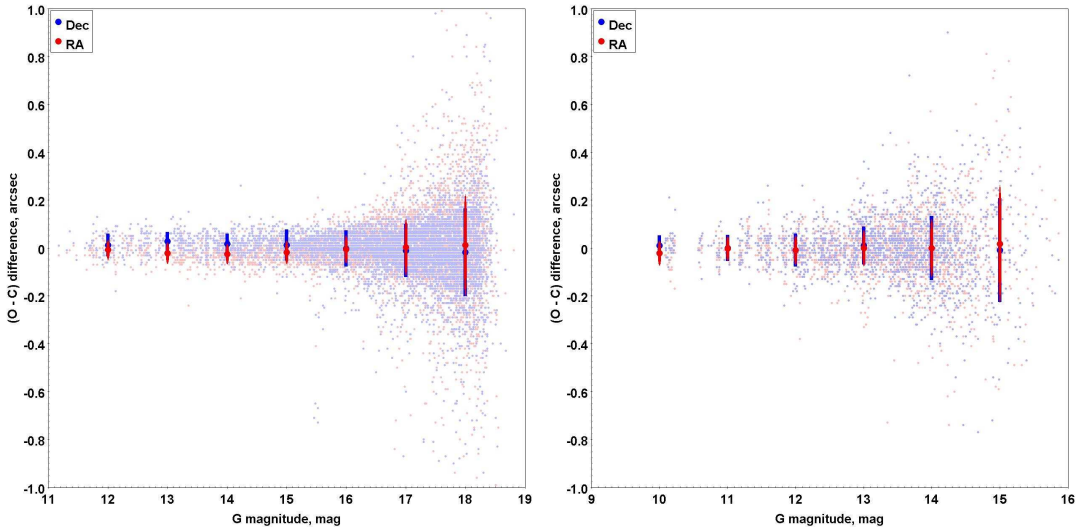

Fig. 2: Mean values of (O – C) differences in reference stars positions regarding to magnitude in $GaiaDR2$ system with one sigma interval error bars: LiShan telescope, NTSC (left); KT-50 telescope, RI MAO (right).

It worth noting, during taking observations of the objects (middle CCD frames of the observational sets with exposures range in 25 - 150 s) there are cases when pointed image of the object crosses trailed image of a star. Such frames are excluded from processing.

4 RESULTS AND PRECISION ANALYSIS

The regular observations of asteroids at LiShan telescope (code O85) using the RDS CCD technique started at the end of 2019. More than 500 observations of 35 NEAs and 4 asteroids of Main Belt (MBA) were obtained. The MBAs were observed in order to apply of IAU MPC observatory code. The observations of NEAs at KT-50 telescope (code 089) started in 2011 and since then about 8000 positions of more than 400 asteroids were obtained. including more than 3100 positions of 145 PHAs. Unfortunately, weather conditions and the location of the telescope KT-50 significantly restrict the potential and effectiveness of observations. Statistical information of last 3 years of the NEAs observations at LiShan and KT-50 telescopes is shown in Table 2, where N1, N2 number of obtained positions and asteroids, correspondingly; n1, n2 number of the positions and asteroids for newly discovered objects in the current year; (O – C) represents the mean residuals between O – observed positions and C – positions from NEODyS-2 ephemeris[5] on the time of observations and their standard deviation values - σ.

As can be seen from the Table 2, the number of observations obtained by the RDS CCD technique is a small percentage of the growing volume of observations carried out by large monitoring projects such as *Catalina Sky Survey* (more than 150,000 per year) *Pan-STARRS* (more than 300,000 per year) and others (observational statistics[1]). But it should be noted that most of these positions were obtained in the period of CA to the Earth, when the asteroids moved with a high apparent velocities in the FOV and, as a rule, they were little observed by other observers in classical modes. Observations of newly discovered (n1, n2) asteroids are especially important in this period in order not to lose them in the next

[5]NEODyS-2: Near Earth Objects - Dynamic Site, *http://newton.dm.unipi.it/neodys/*

Table 2: NEAs observation statistics of the RI MAO (code 089) and LiShan station (code O85)

Year	IAU MPC code	N1	N2	Current year		(O – C) σ, $''$	
				n1	n2	RA	Dec
2017	089	664	32	246	12	-0.00 0.16	0.06 0.19
2018	089	915	45	200	12	0.03 0.18	0.09 0.21
2019	089	823	34	121	7	0.02 0.20	0.02 0.23
2019	O85	395	14+4	54	2	-0.01 0.12	0.08 0.13
2020*	089	1108	28	23	4	0.01 0.17	-0.01 0.21
2020*	O85	289	21	12	1	-0.01 0.16	0.04 0.18

** Data regarding on 2020 November*

period of visibility. For example, asteroid *2019 JL3* was first observed by Mt. Lemmon Survey on 2019 May 8[1]. Its CA to the Earth was on 2019 May 20 with minimal distance 0.006 AU and apparent motion was $105.29''$ min^{-1} (42.12 deg day^{-1}). Last optical observation before the CA moment was obtained on May 12. The total number of observations presented in IAU MPC database at that time was only 55 positions. RI MAO observations at KT-50 telescope have been performed on 2019 May 20. Comparison of the obtained observations with current JPLs HORIZONS ephemeris has shown large differences, which significantly decreased when these observations were added to the IAU MPC database. Table 3 shows values of the (O – C) differences for the KT-50 observations of *2019 JL3* with JPLs HORIZONS ephemeris, which calculated on May 20 **(1)** and in a few days after this date **(2)**, when the observations were added to IAU MPC database.

Table 3: *2019 JL3* (O – C) differences (code 089)

Date	(O – C),$''$ (1)		(O – C),$''$ (2)	
2019.05	RA	Dec	RA	Dec
20.000335	-0.98	0.30	-0.13	-0.06
20.005732	-0.92	0.37	-0.08	0.01
20.011136	-0.80	0.22	0.04	-0.15
20.016528	-0.74	0.33	0.09	-0.00
20.019223	-0.69	0.58	0.14	0.22
20.021921	-1.17	0.28	-0.35	-0.08
20.024617	-0.92	0.55	-0.10	0.17
Mean	**-0.89**	**0.38**	**-0.06**	**0.02**
σ	**0.16**	**0.14**	**0.17**	**0.13**

The JPLs HORIZONS ephemeris system has been used to get ephemeris position of the objects for calculation of (O – C) differences. The mutual distribution of all NEAs mean (O – C) differences in right ascension and declination is shown in Figure 3 for LiShans (code O85) 2019-2020 observations (left) and Mykolaivs (code 089) 2017-2020 observations (right).

Many of these asteroids have poorly determined orbits and as the results the (O – C) differences can deviate from zero significantly. Therefore, the scatter of these differences (standard deviation) will be the more accurate assessment of the precision of the observations. The standard deviation σ of the (O

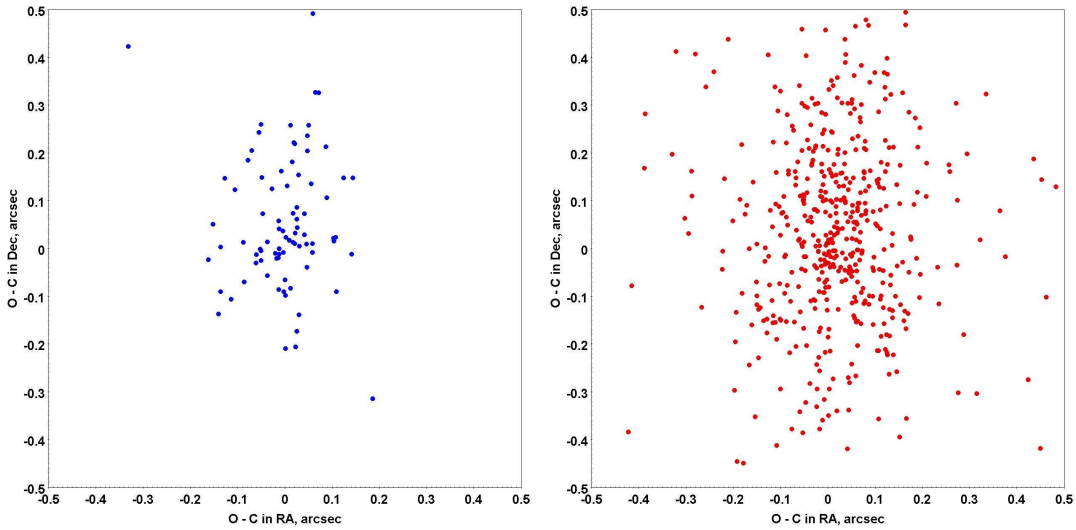

Fig. 3: The mutual distribution of mean (O - C) differences in right ascension and declination for LiShans (code O85) 2019-2020 observations (left) and Mykolaivs (code 089) 2017-2020 observations (right).

– C) differences for NEAs observations at one observational set are shown in Figure 4 versus apparent magnitude.

As can be seen from Figure 3 and Figure 4, precisions of NEAs Mykolaiv observations are high enough for this kind of objects. Mean values of the (O – C) differences with its standard deviation for right ascension and declination are -0.01″ 0.14″ and 0.05″ 0.16″ for LiShan telescope and 0.02″ 0.18″ and 0.03″ 0.21″ for KT-50 telescope respectively.

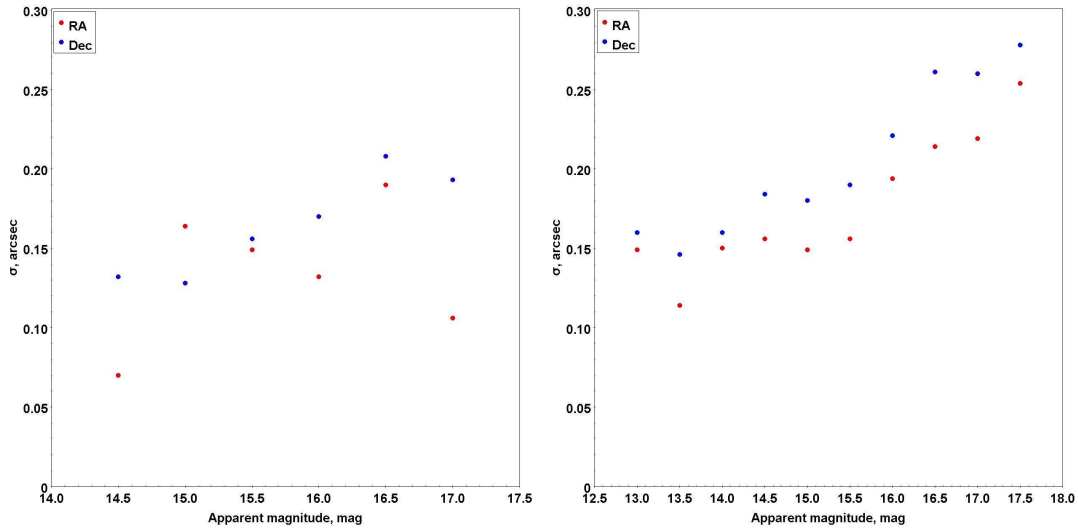

Fig. 4: The mean of standard deviations σ of the (O – C) differences for one observational set of the asteroid is shown plotted against asteroids apparent magnitude. For the asteroids up to 16 mag these errors are less than 0.2″, in both in coordinates. LiShans (code O85) (left); Mykolaivs (code 089) (right).

As noted in Veres et al. (2018), the sufficient precision in orbital elements determination of newly discovered objects will allow us not to lose them in the next orbital turns and CA to the Earth. Despite the large number of observational projects, both professional and amateur, the usage of the RDS CCD technique allows to obtain a significant part of observations of individual objects with sufficient precision. Results of observations for some selected NEAs is given in Table 4, where **N1** and **N2** are number of Mykolaiv observations and total amount of observations in the IAU MPC database, **Mag** mean apparent magnitude. **Uncertainty Parameter** is U parameter of IAU MPC center which describes quantification the uncertainty in a perturbed orbital solution for the asteroids. The column 5 shows the minimal distance to the Earth which specified NEA has reached in the current close approach (**ephem.**) and distance to the Earth on which object have observed by RI MAO (**observ.**). The maximum apparent motion at the time of minimal distance to Earth (**max.**) and during observations at RI MAO (**observ.**) are presented in column 6. Among presented NEAs, the observations made at RI MAO for *2019 JL3* are last before- and *2017 MC4* are first after close approach to Earth in current orbital turn.

Table 4: Results of the selected PHAs observations

NEA	**N1**	**N2**	**Uncert.**	**Min. Dist., *** AU		**App. Motion, **** $''$ min^{-1}		**(O – C)** σ, $''$		**Mag**
			Param.	**ephem.**	**observ.**	**max.**	**observ.**	**RA**	**Dec**	
2019 EA2	22	167	4	0.00205	0.00360	217.21	66.93	0.03 0.25	-0.19 0.39	16.3
2019 JL3	7	60	5	0.00637	0.00649	114.21	105.29	-0.06 0.16	0.01 0.13	16.1
2017 MC4	13	156	2	0.01955	0.02127	87.67	74.61	0.24 0.27	0.00 0.19	16.5
2019 JV1	14	157	6	0.02450	0.03431	59.52	30.79	-0.07 0.25	0.25 0.29	16.5
2019 CD5	6	168	5	0.02597	0.02893	54.25	42.80	0.06 0.14	0.23 0.29	16.5
2018 UQ1	16	254	3	0.02415	0.03718	42.22	17.30	0.12 0.11	0.22 0.13	16.9
2017 YE5	19	346	3	0.03986	0.04060	32.11	30.87	0.07 0.19	-0.03 0.25	16.6
2017 OP68	39	338	4	0.05115	0.05555	18.95	16.14	0.00 0.11	-0.09 0.19	15.6

** Data regarding on current apparition observed at RI MAO (089). The column **ephem.** shows possible minimal distance to Earth regarding to Geocenter; the column **observ.** – regarding to observational site (code 089).*

*** The column **max.** shows maximum apparent motion regarding to Geocenter; the column **observ.** – regarding observational site (code 089)*

As can be seen from the Table 4 the precision of NEAs observations performed by RDS CCD technique doesnt depend on their visible velocity. The RDS CCD technique has potential in observations of NEAs with high apparent motion in order to reach sufficient precision for regular and follow-up observations because currently a large number of observed NEAs are lost subsequently due to inaccurate orbit determination after CA discovery.

In order to compare results presented in current research with world asteroids observations an analysis of statistical information presented on IAU MPC website regarding to precision of asteroids observations has been done. For analysis were chosen observatories or surveys mentioned in Section 1, which make the biggest contribution to asteroids observations including RI MAO (code 089). Only data since 2010 has been analyzed. Unfortunately, the IAU MPC service has stopped provide such statistical data in 2018, so there is no data for LiShan telescope. Table 5 shows averaged (O – C) differences in right ascension and declination (mean) with averaged standard deviation values (mean σ) presented in residuals statistics information of IAU MPC[1] for selected surveys upon considered time period.

The precision of observations of RI MAO is higher than average one for "all observatories" and at the same level with considered observatories/surveys despite of the apparent motion of objects in

Table 5: Averaged by the years statistics of observational precision from IAU MPC database

RA, $''$		Dec, $''$		Observatory IAU MPC code	Observatory name
mean	**mean σ**	**mean**	**mean σ**		
0.00	0.25	0.04	0.26	089	RI MAO
0.06	0.65	0.30	0.62	703, 704	Catalina Sky Survey
0.05	0.54	0.02	0.59	C51	WISE (NEOWISE)
0.03	0.13	0.07	0.14	F51	Pan-STARRS 1
0.02	0.32	0.05	0.29	G96	Mt. Lemmon Survey
0.02	0.47	0.08	0.49	T05, T08	ATLAS-HKO, ATLAS-MLO
0.01	0.48	0.03	0.45	all observatories	

these observations is higher. The Figure 5 shows distribution of apparent speed for mentioned observatories/surveys among the NEAs observations since 2010. The presented comparison shows, in general, observations obtained at KT-50 telescope of RI MAO (code 089) were taken when observed NEAs had higher apparent motion.

It should be noted that the comparison of apparent speed distributions of big surveys with our RDS observations might seem in some measure incorrect from the point of view to the difference in the tasks set. The main tasks of the surveys are monitoring all known asteroids and discovering new ones. The described RDS CCD technique is mainly applicable for targeted observations of fast-moving objects due to the specifics of the observational process based on the apparent motion of the object. The purpose of provided comparison is to show that observations using RDS CCD technique have precision at the comparable level with the best ground-based optical observations of the NEAs.

The usage of the RDS CCD technique gives the opportunity to observe the approaching object at minimal distance to the Earth during high apparent speed. Part of observations carried out in RI MAO in 2017 using RDS CCD technique have index **h** (high precision) according MPC statistics (observational statistics[1]) which indicate reliability of obtained observations and used observational technique.

5 CONCLUSIONS

This paper describes Rotating-drift-scan CCD technique for observations of fast moving PHAs during their CA to the Earth. The technique was implemented on two small-sized parallactic optical telescopes: LiShan telescope of NTSC since 2018 and RI MAO KT-50 telescope since 2011. The results of processing the observations obtained using this technique show that the precision of the positions with respect to the JPLs HORIZONS ephemeris system is in the range $0.1'' - 0.3''$ for the asteroids with apparent magnitudes up to 17 mag. In order to estimate the external precision of presented observations and compare them with the data of other observatories, the IAU MPC statistics results for all observatories over 2010 - 2018 have been used. The analysis of the statistics IAU MPC database shows that this is a good level of precision for observations of such objects. In addition, the ability to obtain pointed images of fast asteroids at moments of CA to the Earth expands the orbit arc, which can be useful for refining the orbital elements and do not to lose this object in the next period of visibility. It is expected decreasing average size of newly discovered NEAs in future thus the detection will be at closer distance to the Earth with higher apparent motion and RDS CCD technique has potential to get observations of such objects with sufficient precision.

Acknowledgements This research is supported by the National Natural Science Foundation of China (Grants No. U1831133 and No. 12073062) and National Astronomical Data Center of China.

References

Evans D. W., Irwin M. J. & Helmer L., 2002, A&A, 395, 347 5
in ASP Conf. Ser. Vol. 43, Sky Surveys., ed., T. B. Soifer (San Francisco: ASP), 267
Gehrels T., McMillan R. S., Scotti J. V. & Perry M. L., 1990, in CCDs in astronomy ASP Conf. Ser., (San Francisco: ASP), 51 3
Harris A. W. & DAbramo G., 2015, Icarus, 257, 302 2
Ivantsov A., Pomazan A., Kryuchkosriy V. & Gudkova L., 2012, Od. Astr. Pub., 25 (1), 66 4
Jedicke R., Granvik M., Micheli M. et al., 2015, in Asteroids IV, eds., P. Michel, et al. (University of Arizona Press, Tucson), 795 2
Jones L. R., Slater C. T., Moeyens J. et al., 2018, Icarus, 303, 181 2
King I., 1983, PASP. 95, 163 4
Kozyrev E. S., Sybiryakova Y. S. & Shulga A. V., 2010, Kosm. Nauka Tehnol., 16 (5), 71 4
Larson S., Brownlee J., Hergenrother C. & Spahr T., 1998, Bull. Am. Astron. Soc., 30, 1037 2
Maigurova N. V., Pomazan A. V. & Shulga A. V., 2018, Od. Astr. Pub., 31, 216 2
Mainzer A., Bauer J., Cutri R. M. et al., 2014, ApJ, 792 (1), 14 2
Shulga A. V., Kozyryev Y. & Sibiryakova Y., 2008, in Proc. IAU Vol. 3, S248: A Giant Step: from Milli- to Micro-arcsecond Astrometry., ed., W. J. Jin et al. (Cambridge Univ. Press online), 128 4
Sybiryakova Y. S., Shulga A. V., Vovk V. S., Kulichenko N. O. & Kozyryev Y., 2015, Kinem. and Phys. of Cel. Bodies, 31 (6), 296 5
Tang Z. H., Pinigin G. & Shulga A. V., 2006, in Proc. of the Intern. Sc. Conf., Enlargement of Collaboration in Ground-Based Astronomical Research in SEE Countries. Studies of the Near-Earth and Small Bodies of the Solar System., ed., G. Pinigin et al. (Mykolaiv: Atoll), 184 3
Tang Z. H., Mao Y. D., Li Y. et al., 2014, Mem. S. A. It., 85, 821 3
Tonry J. L., Denneau L., Heinze A. N. et al., 2018, PASP, 130, id.064505 2
Tricarico P., 2017, Icarus, 264, 416 2
Trilling D.E., Valdes F., Allen L. et al., 2017, AJ, 154, id.170 2
Veres P., Payne M., Holman M. et al., 2018, AJ, 156 (1), 5 3, 9
Wainscoat R. J., Weryk R. C. & Kenneth C., 2018, AAS Meeting #231, id.115.05 2

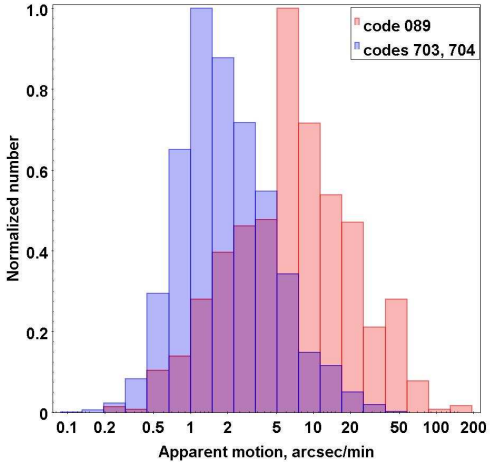

(a) $2.98\,''\ \mathrm{min}^{-1}$ $3.67\,''\ \mathrm{min}^{-1}$

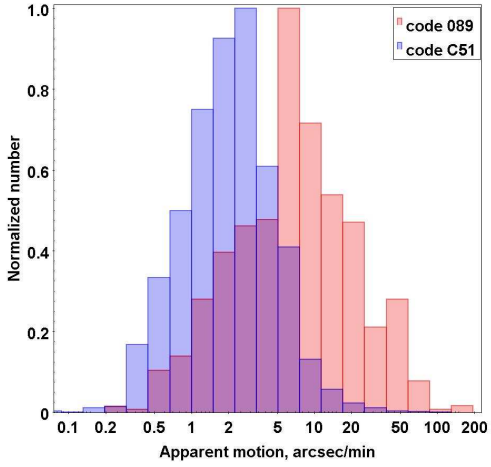

(b) $2.85\,''\ \mathrm{min}^{-1}$ $3.49\,''\ \mathrm{min}^{-1}$

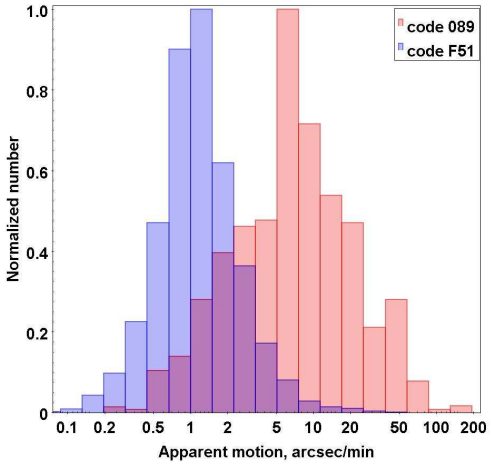

(c) $1.59\,''\ \mathrm{min}^{-1}$ $2.04\,''\ \mathrm{min}^{-1}$

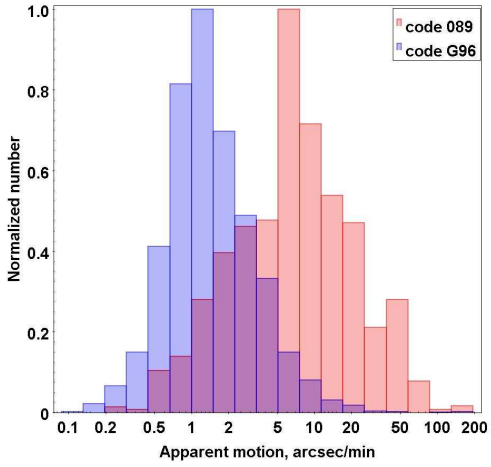

(d) $2.26\,''\ \mathrm{min}^{-1}$ $8.40\,''\ \mathrm{min}^{-1}$

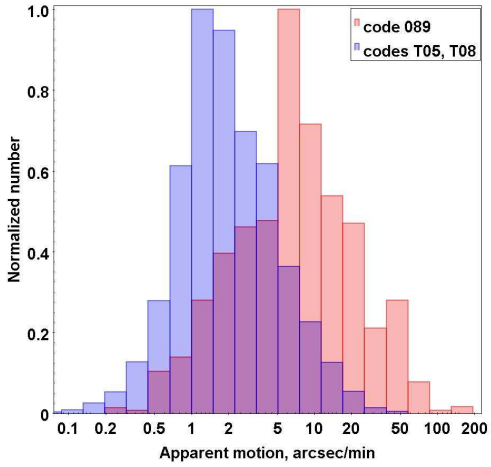

(e) $1.59\,''\ \mathrm{min}^{-1}$ $2.04\,''\ \mathrm{min}^{-1}$

Fig. 5: The distribution of apparent motion for NEAs' observations since 2010 for selected observatories/surveys in comparison to observations of RI MAO (code 089). The mean value of apparent motion and its standard deviation for compared observatory/survey are given in the title of each part; for RI MAO observations mean and standard deviation are $11.84\,''\ \mathrm{min}^{-1}$ $14.94\,''\ \mathrm{min}^{-1}$